Electronic Supplementary Information

Synergistic Modulation of Electronic Structure in PtCo Intermetallic Electrocatalysts via N, F-Co-doped Graphene for Durable Oxygen Reduction Reaction

Zhihao Wang[a,b]†, Wenqiang Li[c]†, Zibo Chen[a], HuiHui Jin[d], Yunfa Si[a], Xiaodong Ji[a], Lun Li[b], Cheng Chen[a,e]* and Daping He[a,d]**

[a] Sanya Science and Education Innovation Park of Wuhan University of Technology, Sanya 572000, China

[b] School of Materials Science and Engineering, Wuhan University of Technology, Wuhan 430070, China

[c] College of Chemistry and Chemical Engineering, Luoyang Normal University, Luoyang 471934, PR China

[d] Hubei Engineering Research Center of RF-Microwave Technology and Application, School of Science, Wuhan University of Technology, Wuhan 430070, China

[e] State Key Laboratory of Advanced Technology for Materials Synthesis and Processing, Wuhan University of Technology, Wuhan 430070, China

**E-mail: jinhuihui@whut.edu.cn, chengchen@whut.edu.cn, hedaping@whut.edu.cn*

† These authors contributed equally to this work.

Experimental Section

Material Characterization

Powder X-ray diffraction (XRD) patterns were collected using a diffractometer with Cu Kα radiation (λ = 1.5406 Å) (Bruker D8 Advance). A JSM-7100F scanning electron microscope (SEM) facilitated the electron microscopy analysis. Data were acquired utilizing a JEM-2100F system for transmission electron microscopy (TEM) and high-resolution transmission electron microscopy (HR-TEM). The high-angle annular dark field scanning transmission electron microscopy (HAADF-STEM) was executed on a transmission electron microscope equipped with spherical aberration correction, specifically a JEOL ARM 200F. Spectral data from Raman were obtained using a Renishaw (INVIA) system, where an Ar ion laser served as the source of excitation light, adjusted to an excitation wavelength of 514.5 nm. An ESCALAB 250Xi spectrometer was utilized to conduct X-ray photoelectron spectroscopy (XPS) with Al-Kα radiation (1486 eV). The Brunauer-Emmett-Teller (BET) method was employed to assess specific surface areas via N_2 physisorption using a Micromeritics ASAP 2020 device.

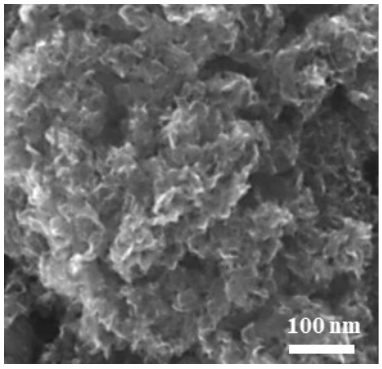

Fig. S1 SEM image of GC.

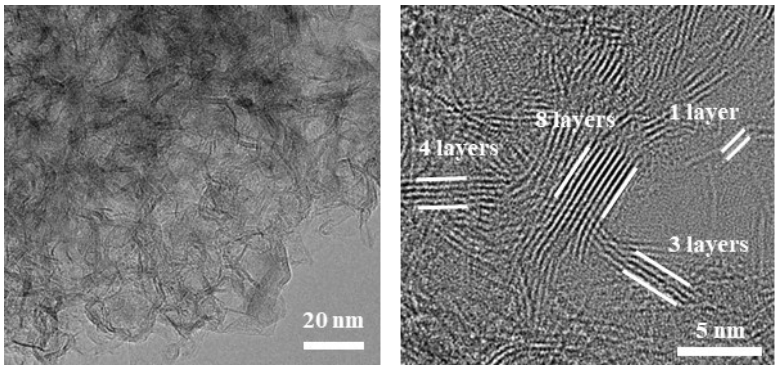

Fig. S2 TEM and HRTEM images of GC.

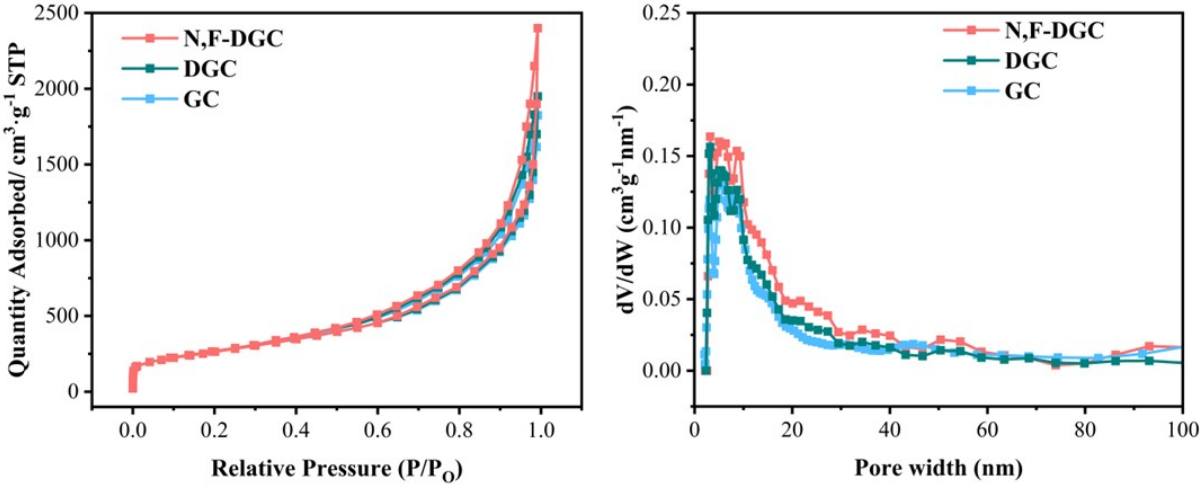

Fig. S3 N_2 adsorption-desorption isotherms and pore-size distribution of GC, DGC and N, F-DGC.

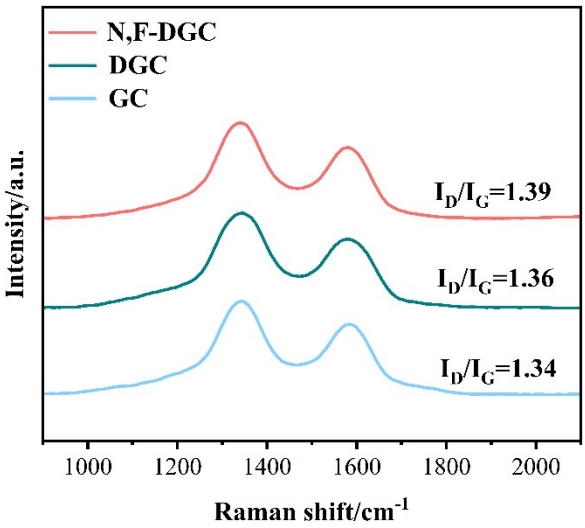

Fig. S4 Raman spectra of GC, DGC and N, F-DGC.

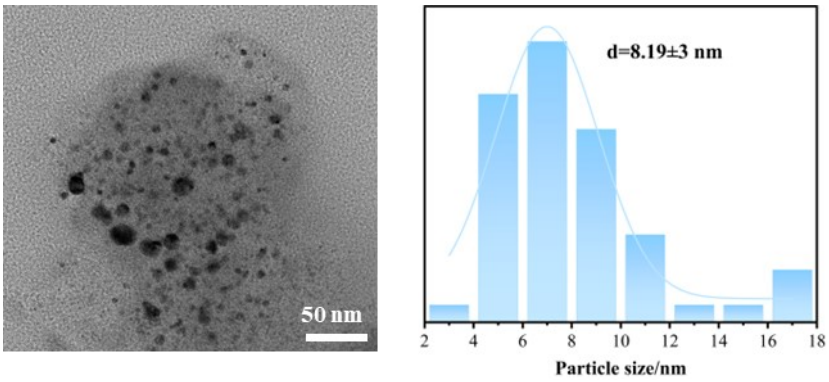

Fig. S5 TEM image and particle sizes analysis of PtCo/DGC.

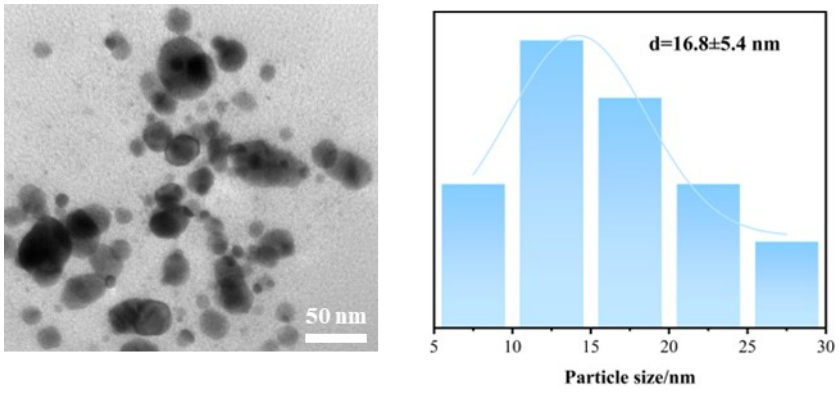

Fig. S6 TEM image and particle sizes analysis of PtCo/GC.

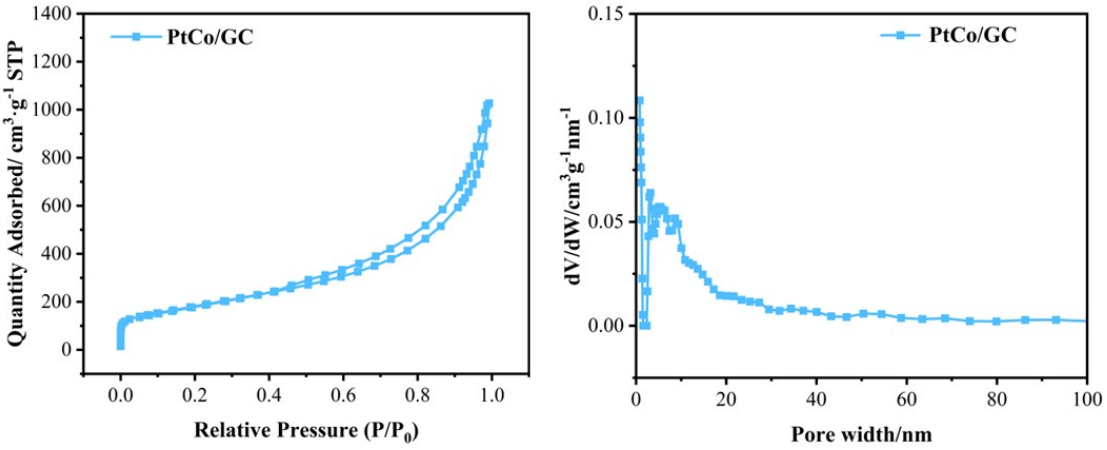

Fig. S7 N_2 adsorption-desorption isotherms and pore-size distribution of PtCo/GC.

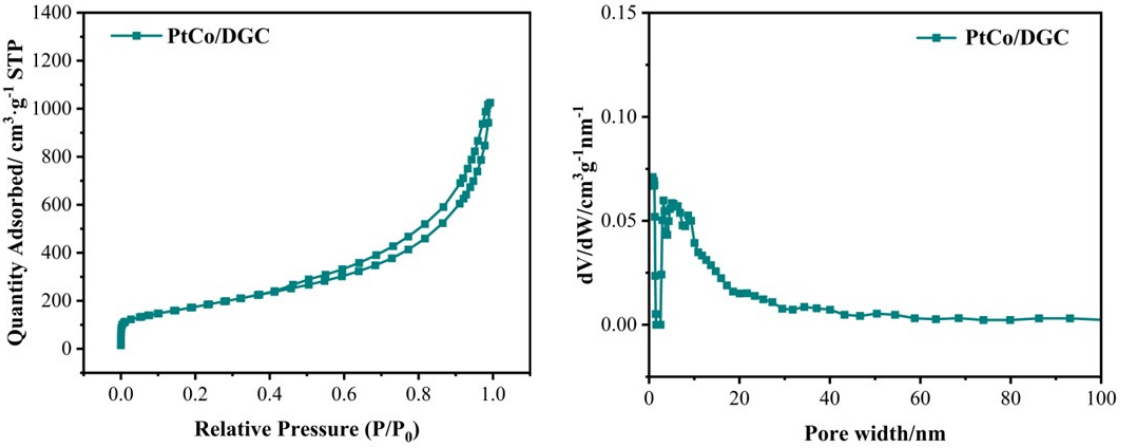

Fig. S8 N_2 adsorption-desorption isotherms and pore-size distribution of PtCo/DGC.

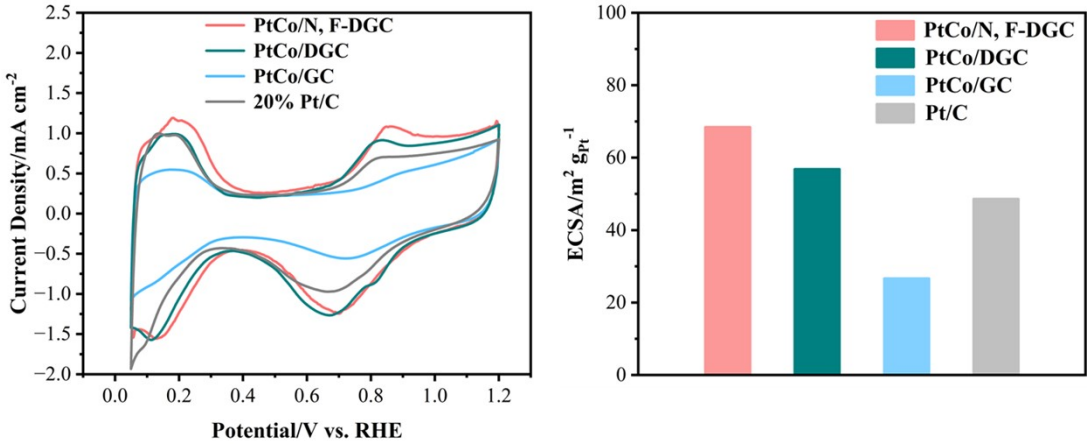

Fig. S9 Comparison of CV curves of PtCo/N, F-DGC, PtCo/DGC, PtCo/GC and commercial Pt/C.

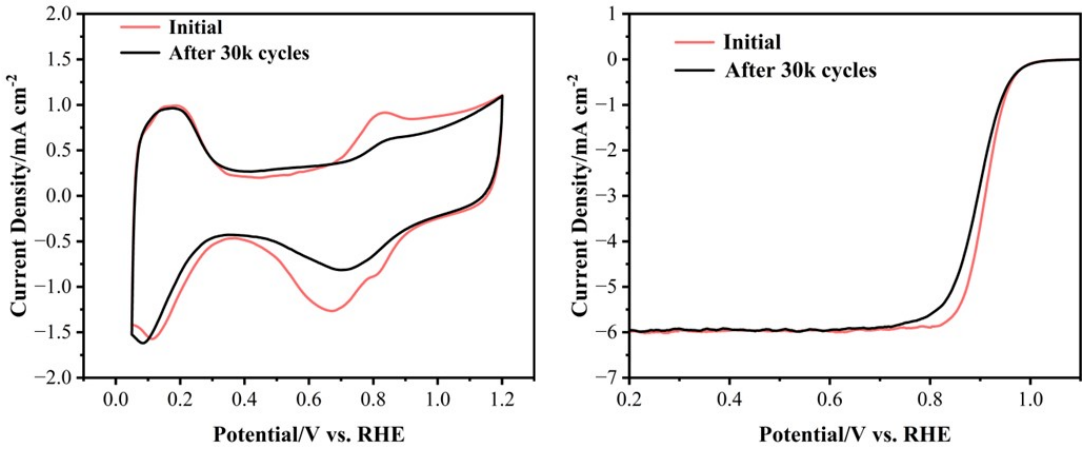

Fig. S10 CV and LSV curves of PtCo/DGC before and after 30k cycles.

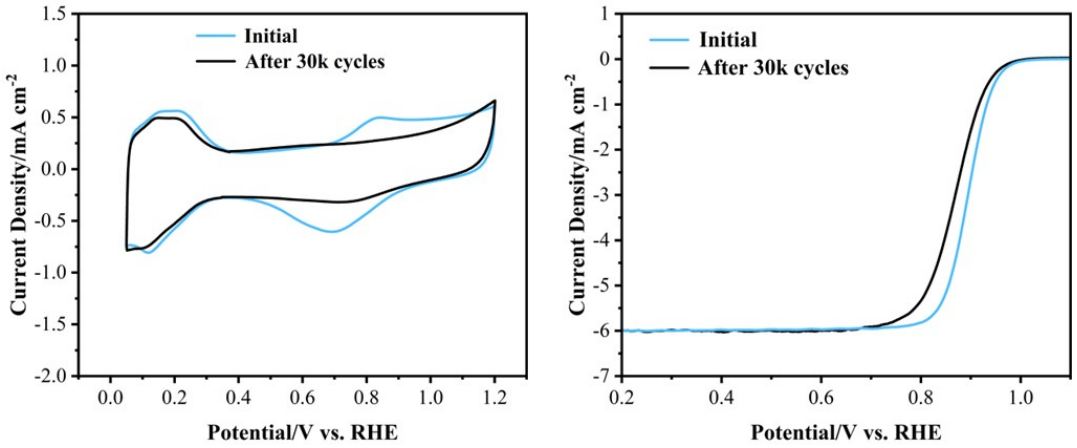

Fig. S11 CV and LSV curves of PtCo/GC before and after 30k cycles.

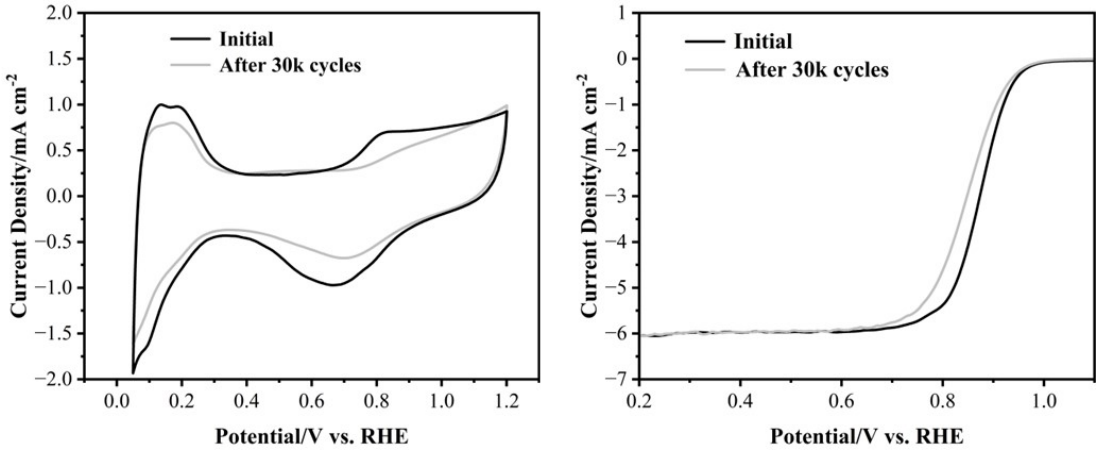

Fig. S12 CV and LSV curves of Pt/C before and after 30k cycles.

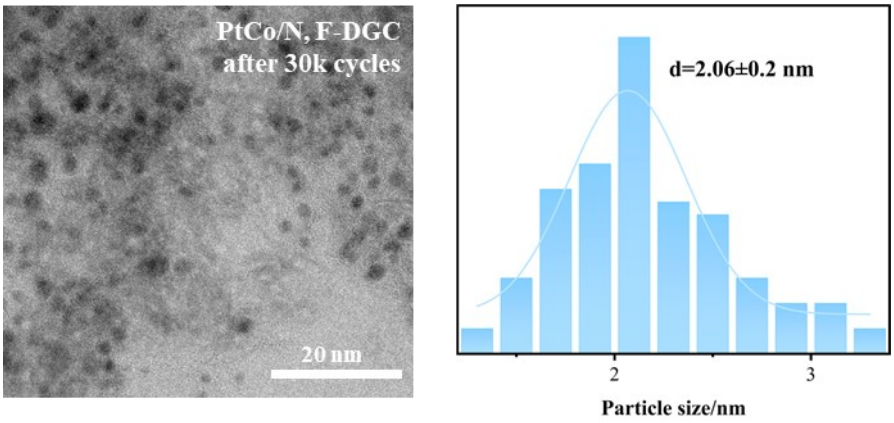

Fig. S13 TEM image and particle sizes analysis of PtCo/N, F-DGC after 30k cycles.

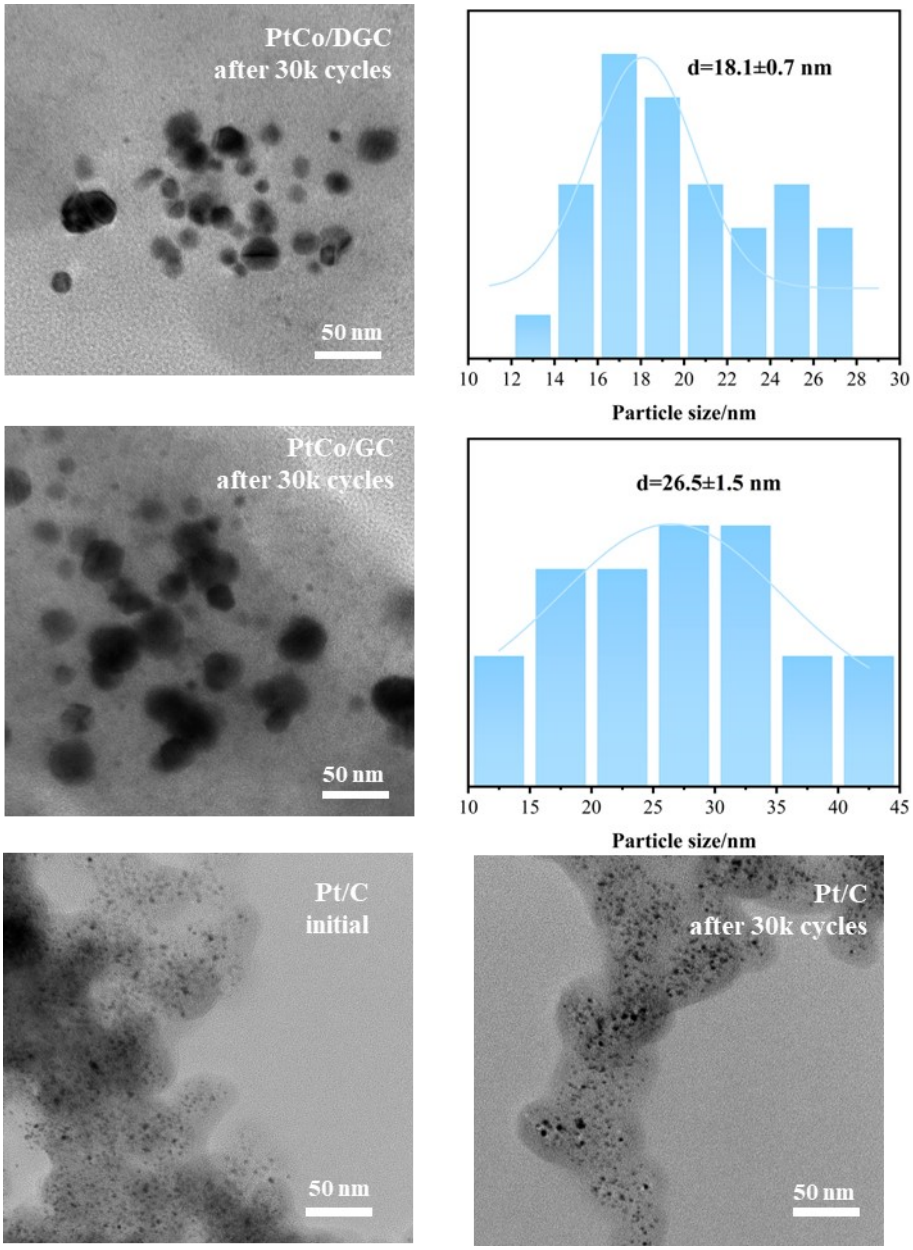

Fig. S14 TEM images and particle sizes analysis of PtCo/ DGC, PtCo/GC after 30k

cycles and TEM images of Pt/C before and after 30k cycles.

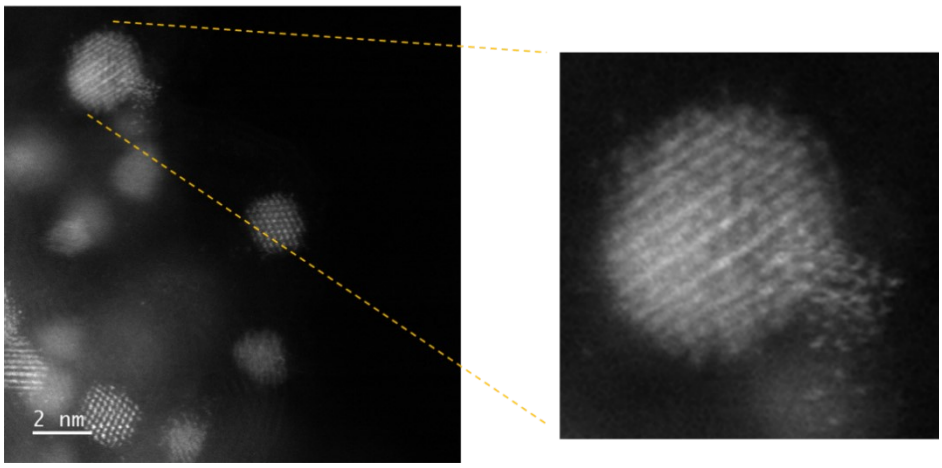

Fig. S15 Atomic-resolution HAADF-STEM image of PtCo/N, F-DGC after 30k cycles.

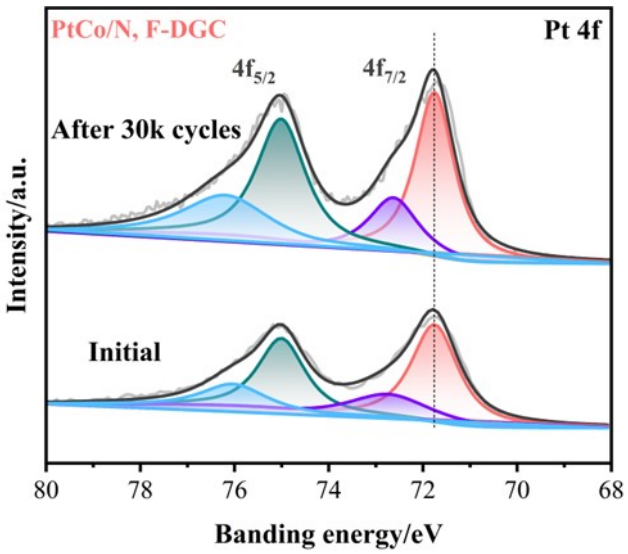

Fig. S16 High-resolution Pt 4f XPS spectra of PtCo/N, F-DGC before and after 30k ADT cycles.

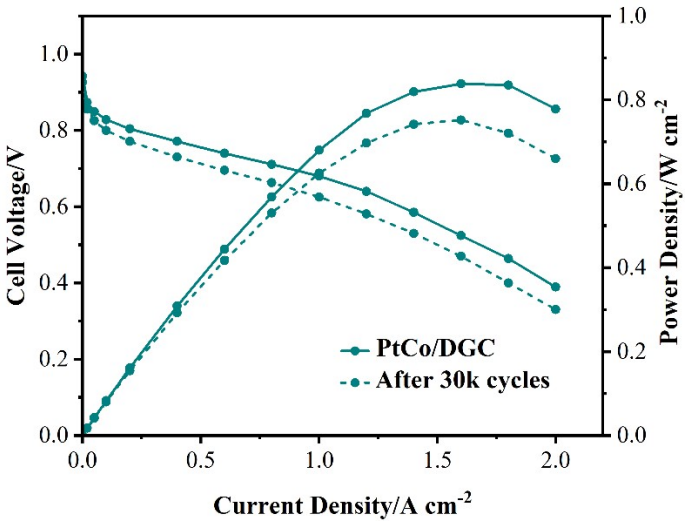

Fig. S17 Polarization curves of H_2-air fuel cell with PtCo/DGC as the cathode before and after 30k cycles.

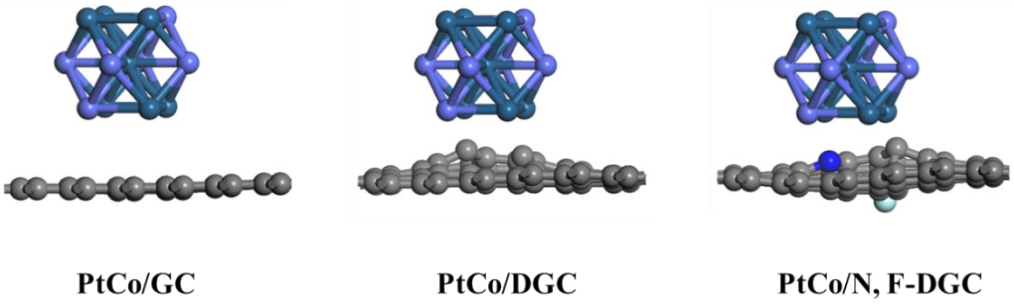

Fig. S18 Optimized atomic structure models.

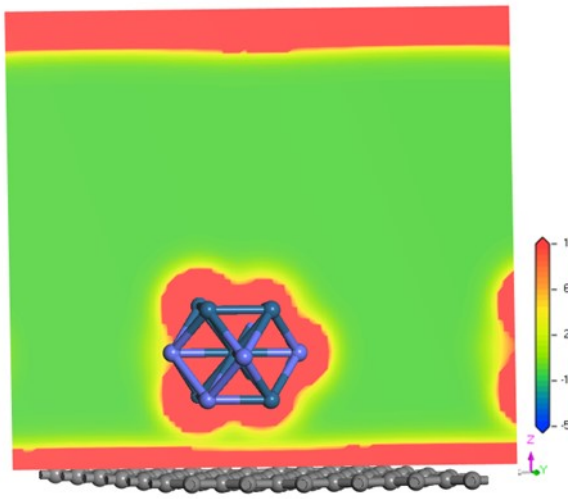

Fig. S19 Differential charge density of PtCo/ GC.

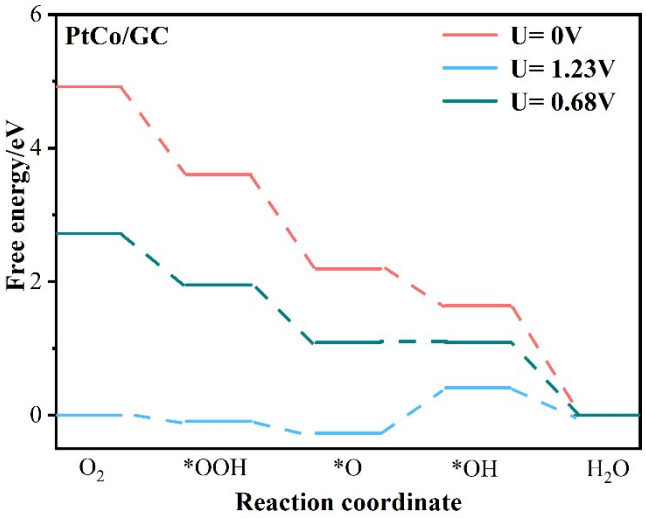

Fig. S20 Calculated free energy evolution along the four-electron associative ORR pathway on the atomic models of PtCo/GC under electrode potentials of 0 V, 1.23 V, and limiting potential.

Table S1. ICP-OES content of all pertinent elements in the corresponding samples.

Sample	Pt (wt.%)	Co (wt.%)
PtCo/GC	16.5	2.73
PtCo/DGC	16.4	2.76
PtCo/N, F-DGC	16.4	2.75

Table S2. Comparison of ORR activity and durability of the catalyst described in this work with the representative Pt-based catalysts reported in the literature.

catalyst	$E_{1/2}$ (V) initial	MA (A mg_{Pt}^{-1}) initial	Loss of $E_{1/2}$ (mV) after 30k cycles	MA (A mg_{Pt}^{-1}) after 30k cycles	MA retention	reference
PtCo/N, F-DGC	0.934	1.02	2	0.88	86.3%	this work
commercial Pt/C	0.873	0.1	25	0.045	55%	this work
Pt@MnSA-NC	0.915	0.63	4	0.49	78%	(1)
PtCo@NGNS	0.95	1.29	20	1.05	81.4%	(2)
FePt@PtBi	0.921	0.96	/	0.79	82.3%	(3)
700-Pt1Co1-IMC@Pt/C-2.5	/	0.53	10	0.41	76.6%	(4)
Surf-IM-PtFe NWs/C	0.956	0.49	3	0.43	87.8	(5)
$PtCu_3$/C	0.945	1.06	27	0.42	40%	(6)
PtCo/Co @NHPCC	0.883	0.57	19	0.36 (5k cycles)	62.7%	(7)
Pt/Co_{SA}-N-C	0.923	0.72	14	0.55 (20k cycles)	75.8%	(8)
O-$PtCo_3$@HNCS	0.909	0.54	/	0.5	92.6%	(9)

Table S3. Comparison of catalytic performance of PtCo/N, F-DGC and previously reported Pt-based catalysts in H_2/air fuel cells.

catalyst	Anode/Cathode loading (mg_{Pt} cm^{-2})	Peak power density (W cm^{-2})	Voltage loss @0.8A cm^{-2} (mV)	reference
PtCo/N, F-DGC	0.1/0.1	0.99	14	this work
Pt@MnSA-NC	0.1/0.1	0.86	10	(1)
i-CoPt@Pt/KB	0.1/0.1	1.27	29	(10)
CoZ-60Pt	0.1/0.2	0.923	/	(11)
O-PtCo@GCoNC	0.1/0.12	1.04	28	(12)
$Ga_{0.1}$-PtCo	0.1/0.075	1.2	27	(13)
Pt_1Fe_1/Fe_1-N-C	0.1/0.1	0.879	/	(14)
$L1_0$-N-PtCo-H@Pt/C	0.05/0.1	0.96	22	(15)
PtCo@Gnp	0.04/0.06	0.92	18.8	(16)

Reference

[1] Y. Zeng, J. Liang, C. Li, Z. Qiao, B. Li, S. Hwang, N. N. Kariuki, C. -W. Chang, M. Wang, M. Lyons, S. Lee, Z. Feng, G. Wang, J. Xie, D. A. Cullen, D. J. Myers and G. Wu, Regulating Catalytic Properties and Thermal Stability of Pt and PtCo Intermetallic Fuel-Cell Catalysts via Strong Coupling Effects between Single-Metal Site-Rich Carbon and Pt, *J. Am. Chem. Soc.,* 2023, **145**, 17643-17655.

[2] S. Zaman, Y.-Q. Su, C.-L. Dong, R. Qi, L. Huang, Y. Qin, Y.-C. Huang, F.-M. Li, B. You, W. Guo, Q. Li, S. Ding and B. Y. Xia, Scalable Molten Salt Synthesis of Platinum Alloys Planted in Metal-Nitrogen-Graphene for Efficient Oxygen Reduction, *Angew. Chem. Int. Ed.,* 2022, **61**, e202115835.

[3] J. Guan, S. Yang, T. Liu, Y. Yu, J. Niu, Z. Zhang and F. Wang, Intermetallic FePt@PtBi Core-Shell Nanoparticles for Oxygen Reduction Electrocatalysis, *Angew. Chem. Int. Ed.,* 2021, **60**, 21899-21904.

[4] Q. Cheng, S. Yang, C. Fu, L. Zou, Z. Zou, Z. Jiang, J. Zhang and H. Yang, High-loaded sub-6 nm Pt1Co1 intermetallic compounds with highly efficient performance expression in PEMFCs, *Energy Environ. Sci.,* 2022,**15**, 278-286.

[5] Y. Ma, J. Peng, J. Tian, W. Gao, J. Xu, F. Li, P. Tieu, H. Hu, Y. Wu, W. Chen, L. Pan, W. Shang, P. Tao, C. Song, H. Zhu, X. Pan, T. Deng and J. Wu, Highly stable and active catalyst in fuel cells through surface atomic ordering, *Sci. Adv.,* 2024, **10**, eado4935.

[6] X. Li, L. Fu, L. Cao, L. Lei, X. Zhan, C. Hu, X. Tong and J. Tian, High electrocatalytic activity of crystallization-modulated ordered $PtCu_3$/C nanoalloy catalysts for oxygen reduction reaction, *Chem. Eng. J.,* 2025, **507**, 160445.

[7] Y. Ying, G. Jiang, Z. P. Cano, Z. Ma, C. Zhong, D. Su and Z. Chen, Metal-organic frameworks derived platinum-cobalt bimetallic nanoparticles in nitrogen-doped hollow porous carbon capsules as a highly active and durable catalyst for oxygen reduction reaction, *Appl. Catal. B Environ.,* 2018, **225**, 496-503.

[8] J. Long, X. Zheng, B. Wang, C. Wu, Q. Wang and L. Peng, Improving the electrocatalytic performances of Pt-based catalysts for oxygen reduction reaction via strong interactions with single-CoN_4-rich carbon support, *Chin. Chem. Lett.,* 2024, **35**, 109354.

[9] Y. Hu, X. Guo, T. Shen, Y. Zhu and D. Wang, Hollow Porous Carbon-Confined Atomically Ordered $PtCo_3$ Intermetallics for an Efficient Oxygen Reduction Reaction, *ACS Catal.,* 2022, **12**, 5380-5387.

[10] T. Y. Yoo, J. Lee, S. Kim, M. Her, S.-Y. Kim, Y.-H. Lee, H. Shin, H. Jeong, A. K. Sinha, S.-P. Cho, Y.-E. Sung and T. Hyeon, Scalable production of an intermetallic Pt-Co electrocatalyst for high-power proton-exchange-membrane fuel cells, *Energy Environ. Sci.,* 2023, **16**, 1146-1154.

[11] W. Zhu, Y. Pei, H. Liu, R. Yue, S. Ling, J. Zhang, X. Liu, Y. Yin and M. D. Guiver, Space Confinement to Regulate Ultrafine CoPt Nanoalloy for Reliable

Oxygen Reduction Reaction Catalyst in PEMFC, *Adv. Sci.,* 2023, **10**, 2206062.

[12] B. Wu, H. Yang, L. Li, X. Tang, Y. Wu, B. Huang, D. Lützenkirchen-Hecht, M. Qiu, K. Yuan and Y. Chen, Integrating PtCo Intermetallic with Highly Graphitized Carbon Toward Durable Oxygen Electroreduction in Proton Exchange Membrane Fuel Cells, *Adv. Mater.,* 2025, **37**, 2500096.

[13] R.-Y. Shao, X.-C. Xu, Z.-H. Zhou, W.-J. Zeng, T.-W. Song, P. Yin, A. Li, C.-S. Ma, L. Tong, Y. Kong and H.-W. Liang, Promoting ordering degree of intermetallic fuel cell catalysts by low-melting-point metal doping, *Nat. Commun.* 2023, **14**, 5896.

[14] F. Zhou, Y. Ruan, M. Zhu, X. Gao, W. Guo, X. Liu, W. Wang, M. Chen, G. Wu, T. Yao, H. Zhou and Y. Wu, Coupling Single-Atom Sites and Ordered Intermetallic PtM Nanoparticles for Efficient Catalysis in Fuel Cells, *Small,* 2023, **19**, e2302328.

[15] M. I. Maulana, T. H. Jo, H.-Y. Lee, C. Lee, C. Gyan-Barimah, C.-H. Shin, J.-H. Yu, K.-S. Lee, S. Back and J.-S. Yu, Cobalt Nitride-Implanted PtCo Intermetallic Nanocatalysts for Ultrahigh Fuel Cell Cathode Performance, *J. Am. Chem. Soc.*, 2024, **146**, 30922-30932.

[16] Z. Zhao, Z. Liu, A. Zhang, X. Yan, X. Wang, B. Peng, H. L. Xin, X. Pan, X. Duan and Y. Huang, Graphene-nanopocket-encaged PtCo nanocatalysts for highly durable fuel cell operation under demanding ultralow-Pt-loading conditions, *Nat. Nanotechnol.,* 2022, **17**, 968-975.